

## Article

# An Attended-Free, All-in-One-Go, Automatic Analysis Assistant Software for E-liked Shape Contactless Inductive Power Transfer Device

Yumeng Lan \* and Masafumi Miyatake 

Department of Engineering and Applied Sciences, Sophia University, Tokyo 1028554, Japan

\* Correspondence: lanyumeng0419@eagle.sophia.ac.jp

**Abstract:** This paper presents automatic software for E-liked shaped contactless inductive power transfer (CIPT) device study and design that provides attended-free, multiple-case auto-generating and auto-deploying analysis in one go. It provides visualized and listed results in a design space or for optimizing solutions. To satisfy the demand for static and dynamic charging devices, the software provides specific cores, such as EE-, EI-, IE-, and II-shaped, with or without legs as optional core structures. The software contains three main parts: a user-friendly interface, analytic approaches providing grid analysis that represent the general performance in a designated parameter range, and optimal analysis for multi-objective optimization using a genetic algorithm (GA). The post-analysis processor converts the analysis results to easy-to-read outputs. Users can customize various parameters, such as core type, structural size, circuit configuration, materials, and analysis setting. Automatic functions, such as resistance and compensation calculation, are available for the convenience of the user. By applying one approach, or by combining them in a specific order, the software achieves designs that satisfy the user's demands within the user-provided range. The software is built in Python and collaborates with a finite element method (FEM) solver, which is JMAG in this paper. Some examples are given to demonstrate the performance of the software.

**Keywords:** automation; contactless inductive power transfer; multi-objective optimization



**Citation:** Lan, Y.; Miyatake, M. An Attended-Free, All-in-One-Go, Automatic Analysis Assistant Software for E-liked Shape Contactless Inductive Power Transfer Device. *Energies* **2022**, *15*, 6244. <https://doi.org/10.3390/en15176244>

Academic Editors: Yang Li and Pengcheng Zhang

Received: 29 July 2022

Accepted: 24 August 2022

Published: 26 August 2022

**Publisher's Note:** MDPI stays neutral with regard to jurisdictional claims in published maps and institutional affiliations.



**Copyright:** © 2022 by the authors. Licensee MDPI, Basel, Switzerland. This article is an open access article distributed under the terms and conditions of the Creative Commons Attribution (CC BY) license (<https://creativecommons.org/licenses/by/4.0/>).

## 1. Introduction

Since the first generator was invented by Michael Faraday in 1831, the electromagnetic field has been used as a medium of energy and information and provides us with essential services, anytime and everywhere. Recently, with the rapid development of electric vehicles and smartphones, contactless inductive power transfer (CIPT) technology has become another focus for the utilization of electromagnetic fields. Unlike traditional transformers, whose primary and secondary coil are wound on the same core, the CIPT device is not tightly coupled, since it aims to deliver power between two unconsolidated entities. The isolation of CIPT provides benefits of safe application (electrical isolation), low maintenance (physical isolation), and convenience (high replaceability of the receiving side).

The typical configuration of a CIPT system is shown in Figure 1. The whole system can be separated into primary and secondary parts. The inverter modulates the frequency from the power supply to a desired high frequency in the primary part. A compensatory capacitor is generally required to reduce the capacity of the power supply. In the secondary part, compensation is also excepted for the same reason. Then a rectifier and other regulators are applied to reach the load requirement.

Although a large number of coreless CIPT systems have been developed due to their light weight [1–5], a well-designed core can accumulate more magnetic flux emissions from the primary side to the secondary side, by increasing the magnetic linkage between them. It dramatically increases the power transfer capability by contributing to high mutual inductance [6]. As they are most similar to the traditional transformer, the E core and its

variants are some of the favored core shapes. Many designs have been produced to optimize performance under specific conditions. Researchers have used higher excitation current and resonant frequency to improve the power transferred for trains [7,8]. Unfortunately, thermal and switching losses limit the current level. In [9], several core structures were numerically analyzed and compared with respect to size effectiveness, the coupling coefficient, and efficiency. The authors proposed a design with 5kW output. Using a magnetic reluctance circuit, refs. [10–12] inferred the coupling coefficient, enabling measurement and improvement of the CIPT performance through improved core design. A normalization optimization method was introduced against the lateral and angular misalignment of the CIPT system in [13]; however, scenarios using coil shapes other than round were not discussed. A design process was proposed for a super capacitor load CIPT system in [14] that considered efficiency as the only objective. With the growth of computing capability and the popularity of artificial intelligence, the automatic optimization of CIPT design involving the processing of a massive number of designs becomes achievable. A GA was used for optimizing the CIPT system using an inductive link model, and optimal designs among different numbers of resonators were compared in [15]. However, only the power capacity and system efficiency were taken into consideration in the example used. A tool for automatically optimizing the compensation network was introduced in [16] that introduced a third objective function to evaluate sensitivity to the other objectives, which was capable of ensuring the stability of the system. The tool they proposed defined the objectives as minimum problems limiting its expansibility. The power capacity and efficiency are always priorities for a power delivery system, and CIPT is no exception. Furthermore, the back-end requirement must be met by regulating the output voltage and output current in the desired range. In comparison with a single design to achieve a predetermined objective, the general design method for the core structure is more complicated. For cored CIPT devices, the coupling coefficient is the critical indicator that shows the degree of magnetic linkage between the two sides. Of course, it is necessary to consider limitations of size from cost and usage perspectives. Unquestionably, a comprehensive approach that consists of magnetic (structural) and electrical considerations would simplify the CIPT design process. The finite element method (FEM) is popular for the electromagnetic analysis of CIPT systems. FEM simulation software can visualize the flow of magnetic fields in different mediums—using it as a design tool can avoid unnecessary waste of resources. The steps to design a CIPT system are as follows:

- S1. Produce an initial CIPT design.
- S2. Analyze the design to obtain the self and mutual inductance.
- S3. Calculate and apply compensation.
- S4. Evaluate the compensated design.
- S5. Check the result. Finish if it meets the demands. Refine the design space and go back to S2 if not.

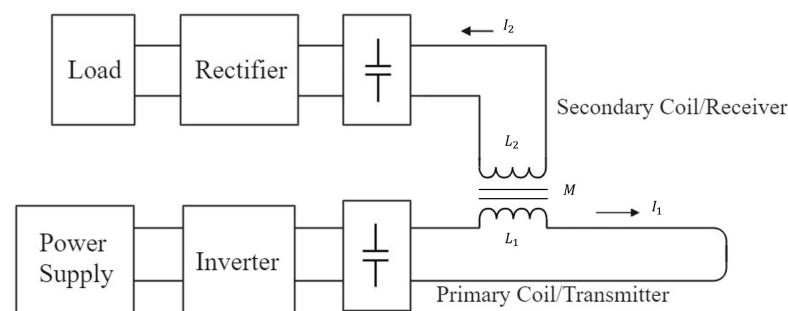


**Figure 1.** Configuration of CIPT system.

Since it is nearly impossible to predict the detailed behavior of the electromagnetic field, the analysis remains a laborious task even with the application of FEM software. At least three analyses are required to verify whether a design thoroughly meets the

requirements. For a large-scale core with a small mesh, the analysis time is often from several hours to days, and more time will be wasted if it is unattended when the previous analysis completes. Between and during each round of analysis (from S1 to S5), calculation and operation are required at least twice (compensation setting and design adjusting). A processor that frees the designer from attendance, handling the data, and which can alter the design for subsequent analysis would undoubtedly be more productive.

This paper presents an automatic software that is capable of shortening the manual operation time with a concentrated and simplified interface and auto-generating, auto-deploying functions. To meet the needs of studying and designing CIPT devices, the software generates approaches for pattern searching and multi-objective optimization. The software is built with the Python language and cooperates with the FEM solver. E-linked core shapes, such as EE, EI, IE, and II, are prepared to address the development requirements of railway CIPT devices, or similar applications, that might be utilized for track charging [17]. The software is capable of calculating the compensation capacitance depending on the chosen topology. Two analysis approaches are implemented, including a grid analysis approach, which emphasizes pattern searching, and an optimization approach, which uses the adjusted non-dominated sorting genetic algorithm II (NSGA-II) to achieve solutions entailing multi-objective optimization. Examples are provided to demonstrate the functions of the software. We expect to identify better solutions, or to consume less time, by using this software to automatically test a large quantity of cases at once.

## 2. Software Configuration

A program is a well-organized assembly of function blocks. The blocks should have clear definitions and be functionally isolated from each other. The proposed software is composed of the following blocks: interface, approaches, and post-analysis operator. The interface block allows the user to customize the parameters, including the global settings, design specifications, and the approach settings. Confirmation and warnings will “pop up” for the user to quickly refine their design space. The analysis approaches section includes grid and optimal methods. The grid method is used for pattern searching with parameter variation in a continuous design space. The optimal approach applies the NSGA-II algorithm with situation-based parameters to determine the optimal solution in a short time. The post-analysis operator oversees the organizing of analysis results into read-friendly tables and figures. The proposed software is compiled in Python and the examples in this paper apply JMAG as the FEM solver.

### 2.1. Interface

To adapt to the diverse demands and purposes of the analysis, the user needs to adjust the solver setting or alter their coding frequently. On the one hand, a considerable amount of time is required to repeat the same steps for skilled users. On the other hand, beginners find it very complicated to get started, which creates significant learning costs. From the viewpoints of productivity and ease of use, in our software, a specialized and simplified interface is applied to achieve rapid configuration.

The interface consists of two parts based on consideration of the parameter variation among different core selections. According to the relative movement between primary and secondary sides, the charging can be classified into static and dynamic methods. For static charging, the coil and core shape mainly depend on the distribution of the electromagnetic field at designated positions, such as aligned and partially misaligned. For dynamic charging, the alternation of performance along the traveling direction must be taken into consideration. One popular method to reduce electromagnetic shifting is to maintain the same cross-section along the traveling direction. The proposed software provides cores composed of E and I shape cores with optional legs, as shown in Figures 2a and 3, due to their ability to operate using both static and dynamic methods. In these figures, the gray parts represent the core area, the green parts stand for the primary coil area, and the yellow parts are the secondary coil area. The I-shaped core does not possess poles and a leg area,

and neither do models without legs have a leg area. Figure 2b presents an example 3D image of a sectioned EE shape with legs structure; the other structures are similar to it without the parts that are not applicable.

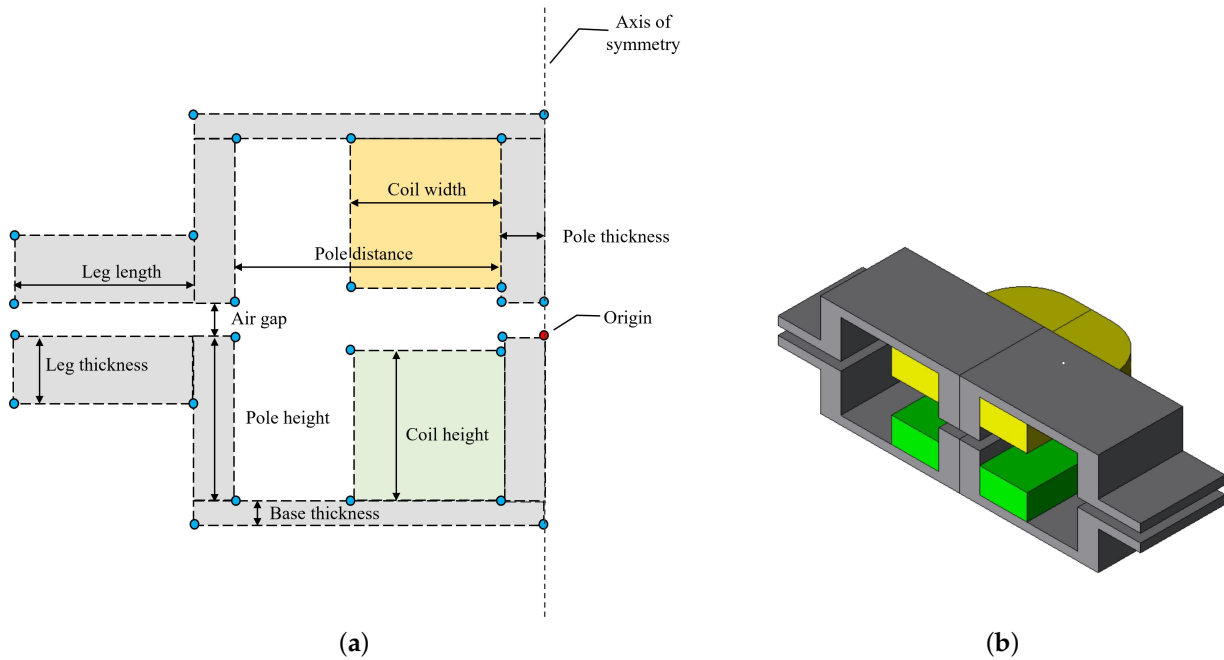


**Figure 2.** Configuration of CIPT device structured as EE shape with legs. (a) is the parts division in 2D and (b) is a sectioned 3D image from the cross-section.

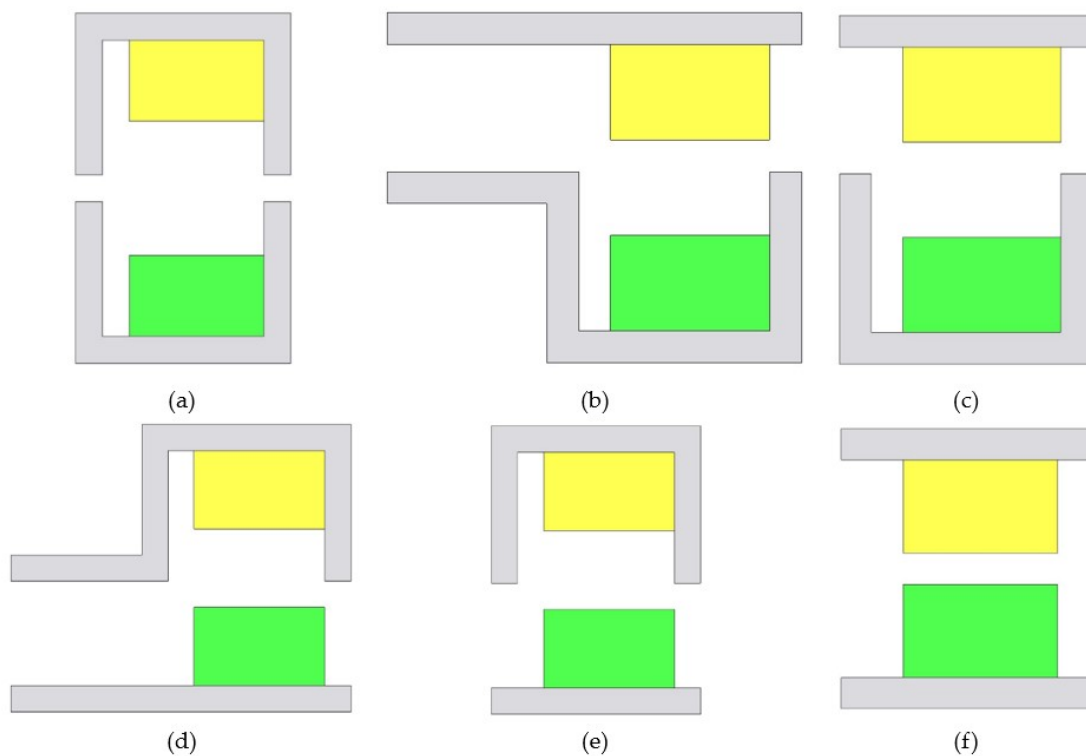


**Figure 3.** Half models (left) of CIPT. (a) EE shape without legs. (b) EI shape with legs. (c) EI shape without legs. (d) IE shape with legs. (e) IE shape without legs. (f) II shape.

As shown in Figure 4, the first window is used for choosing the core shape and FEM solver. The second window is used to define the detailed properties of geometry, circuit, approach, and the FEM-related parameters. The available parameters are dynamically displayed to the user in the second window based on the core shape selection in the previous window. In the geometry section, users can modify the edge of each part of the core and the size of the winding area, as marked in Figure 2. The circuit section allows users to define the operation frequency, component arguments, and compensation topology. In this section, an auto-resistance calculation checkbox is provided as a convenient option. The primary and secondary resistance entries are hidden when checked. After confirmation, the coil resistance is calculated according to the coil-related parameters, assuming the coil is made of Litz wire. Auto compensation is applied when the compensation checkbox is checked. By selecting the primary and secondary sides' capacitance connection in series and parallel, four basic compensation topologies [18–24] as series-series (SS), series-parallel (SP), parallel-series (PS) and parallel-parallel (PP) can be acquired. The material of each part of the model is selectable in the Material&Conditions section and the mesh size is adjustable in the Mesh section.

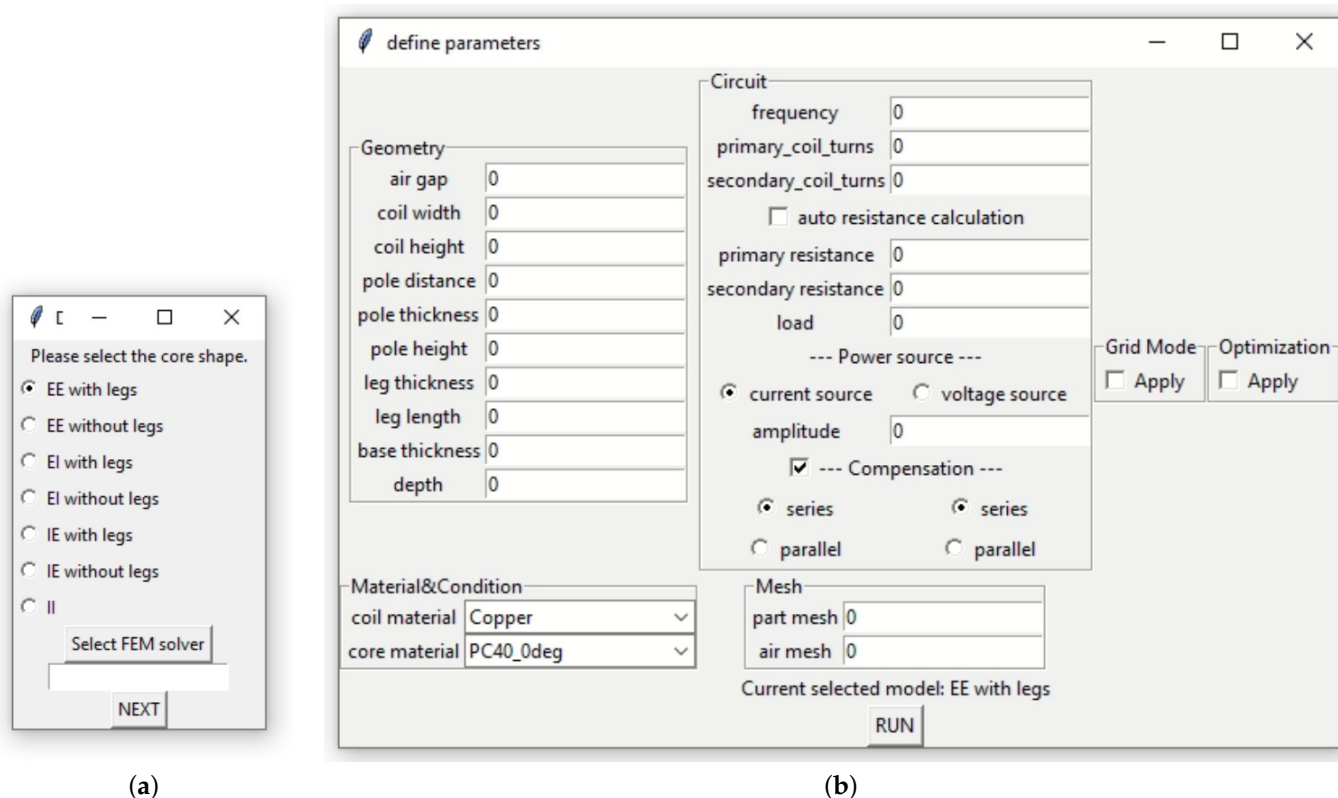


**Figure 4.** The interface of the proposed software. (a) is the core shape and FEM analyzer selection window and (b) is the detailed parameter customization window when EE shape with legs is selected.

As mentioned above, the grid mode and optimization are provided as the analysis approaches. Since they are mutually exclusive, the software only allows one of them to be applied at a time. Both setting sections remain hidden until selected and only the option checked is shown to the user, as shown in Figure 5. The software performs a single analysis using the parameters outside these sections if neither is activated. In the grid mode setting, the interval and end values are required for every checked geometric and circuit parameter. However, the coil resistance setting is not effective when auto resistance calculation is checked in the Circuit section. An interval that is greater than the difference between the start value and the end value triggers a warning that prevents the simulation from launching. In the optimization section, the upper limits of the geometry and circuit

are customizable, the objectives range can be given and GA-related information, such as population and generation, are required. Both approaches use the geometry and circuit inputs in Figure 4 as the lower limits. Meanwhile, compensation is automatically selected when applying the optimization and is highly recommended for grid analysis.

Figure 5 shows two screenshots of a software interface for grid analysis and optimization. Screenshot (a) is titled 'Grid Mode' and features a table for defining parameters with columns for 'interval' and 'end value'. Screenshot (b) is titled 'Optimization' and includes settings for population size, generation number, and various variables with their respective upper limits.

**(a) Grid Mode**

	interval	end value
--- Geometry ---		
<input type="checkbox"/> air gap:	0	0
<input type="checkbox"/> coil width:	0	0
<input type="checkbox"/> coil height:	0	0
<input type="checkbox"/> pole distance:	0	0
<input type="checkbox"/> pole thickness:	0	0
<input type="checkbox"/> pole height:	0	0
<input type="checkbox"/> leg thickness:	0	0
<input type="checkbox"/> leg length:	0	0
<input type="checkbox"/> base thickness:	0	0
--- Circuit ---		
<input type="checkbox"/> amplitude:	0	0
<input type="checkbox"/> primary coil turns:	0	0
<input type="checkbox"/> primary resistance:	0	0
<input type="checkbox"/> secondary coil turns:	0	0
<input type="checkbox"/> secondary resistance:	0	0
<input type="checkbox"/> load:	0	0

**(b) Optimization**

Apply

=== optimization settings ===

population size: 0

generation number: 0

=== variables ===

	upper limit
--- geometry ---	
<input type="checkbox"/> air gap	0
<input type="checkbox"/> coil width	0
<input type="checkbox"/> coil height	0
<input type="checkbox"/> pole distance	0
<input type="checkbox"/> pole thickness	0
<input type="checkbox"/> pole height	0
<input type="checkbox"/> leg thickness	0
<input type="checkbox"/> leg length	0
<input type="checkbox"/> base thickness	0
--- circuit ---	
<input type="checkbox"/> source amplitude	0
<input type="checkbox"/> primary coil turns:	0
<input type="checkbox"/> primary resistance:	0
<input type="checkbox"/> secondary coil turns:	0
<input type="checkbox"/> secondary resistance:	0
<input type="checkbox"/> load:	0
=== objectives ===	
	lower upper
<input type="checkbox"/> output power:	0 0
<input type="checkbox"/> efficiency(%)	0 0
<input type="checkbox"/> coupling coefficient	0 0
<input type="checkbox"/> output voltage	0 0
<input type="checkbox"/> output current	0 0

Figure 5. Approaches interface section. (a) Grid analysis. (b) Optimization.

After clicking on the RUN button, the software runs the validation of the user inputs. The verification section is responsible for assessing the legality of user inputs. The following inputs are considered illegal: non-number, exceeding limitation, violating relative relation, and missing item. Non-number detection checks the contents of all input boxes to ensure that all entry inputs are numbers. Exceeding limitation detection is used to detect whether the input exceeds its inherent range, such as negative inputs and inputs below the lower limit in the approach configuration. Exceeding relative relation refers to exceeding the physical limit between parts. In the E-shape model, the coil area should not exceed the core's inner contour. Otherwise, it is considered to exceed the relative limit. In some cases, missing items, including unselected variables in the approaches and undefined objectives when applying the analysis, can cause failure or produce invalid results, so these need to be identified before the analysis starts. If there is no illegal input, a confirmation pop-up appears with essential information and triggers the subsequent procedure. Otherwise, the pop-up lists the errors in red text for the user to quickly fix. An illustration of pop-up windows is given in Figure 6.

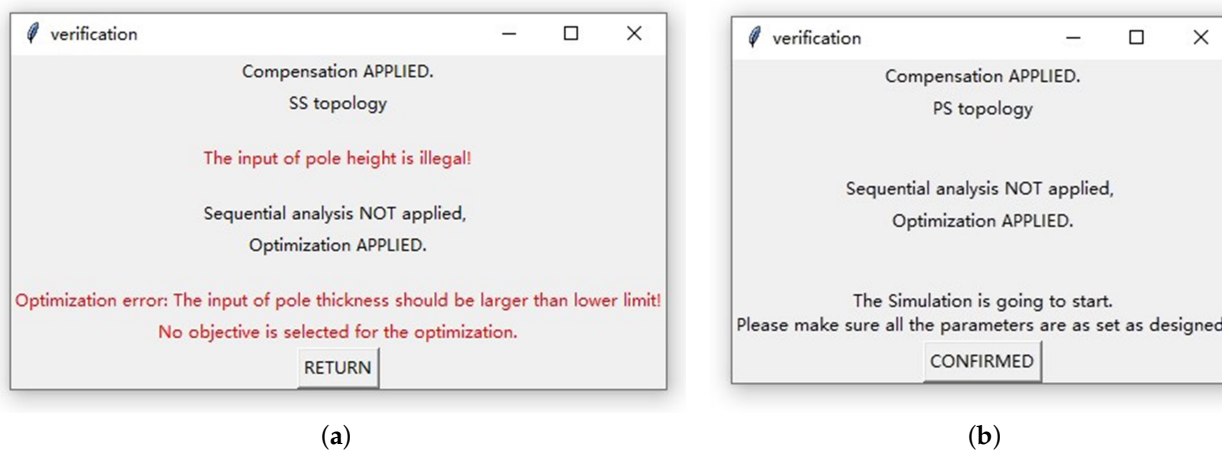


**Figure 6.** Pop-up validation window of (a) warning showing as red lines and (b) confirmation.

## 2.2. Approaches

As mentioned above, the proposed software provides two approaches: grid mode and optimization. According to the parameter limitation and interval defined by the user, the grid mode provides a set of analyses that cover the whole design space. This is mainly to satisfy the demand for pattern searching. The optimization can search for an optimal solution set that meets the objective constraints in the design space. It can handle both single-objective and multi-objective tasks. Theoretically, if there are solutions in the objective range, the optimization can find them with fewer simulations. Both approaches share a part of the process, while their flow is maintained to ensure that the software is compact and fully functional. The shared parts are the pre-analysis data process and analysis status control. A flowchart of these approaches is shown in Figure 7, where the red arrows stand for the grid analysis, the blue arrows are for optimal analysis and the black arrows are for the shared steps. The main application of this software is assumed to be dealing with a large quantity of cases at once; therefore, the FEM analysis involves a 2D model rather than comprehensively constructed 3D models, so that the process does not dry out the storage or take a very long time to finish. By setting the depth of the 2D model, the analysis results can be considered to approximate those using 3D models.

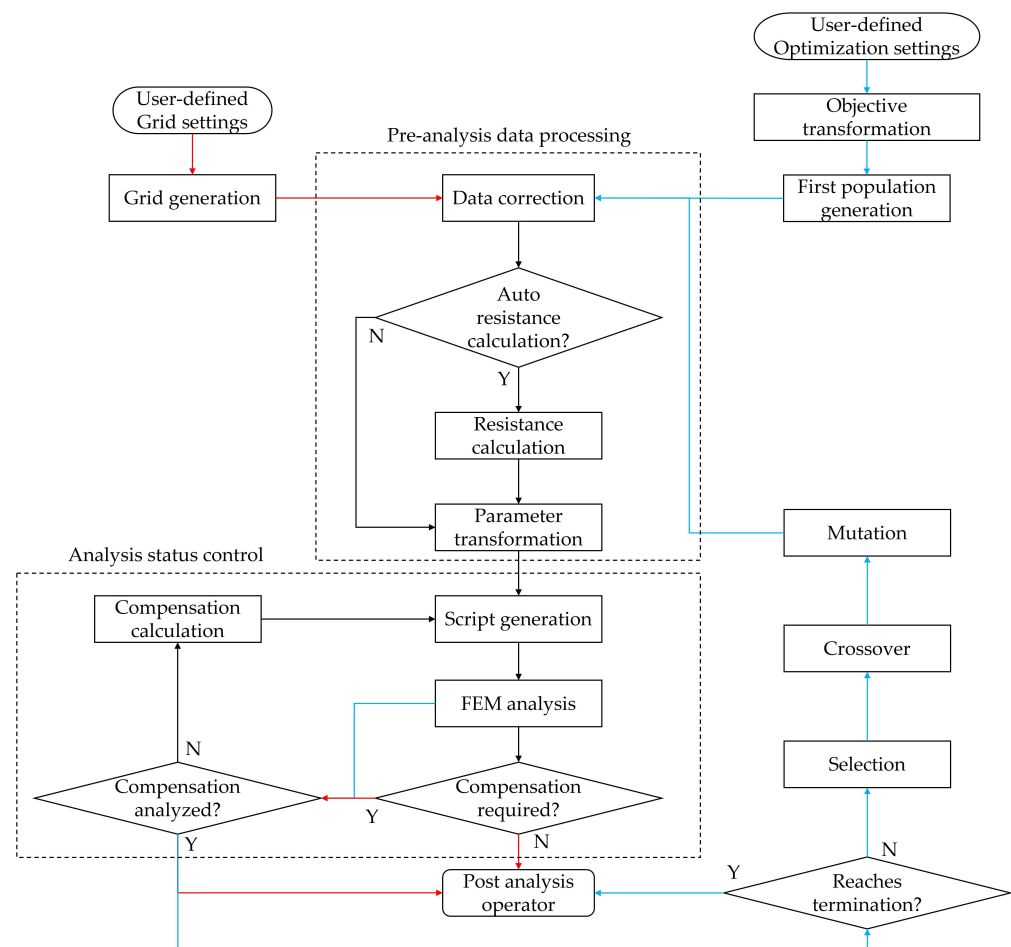


**Figure 7.** Flowchart of the grid and optimal approaches. The red arrows show the flow of the grid approach, the blue arrows for the optimal approaches, and the black arrows as the shared flow.

### 2.2.1. Pre-Analysis Process

The pre-analysis process is designed to guarantee that the data transferred to the analysis block is comprehensive and accurate. It consists of data correction, auto resistance calculation, and parameter transformation stages. In the data correction process, not only are analyses with invalid results removed from the whole analysis, but the candidates waiting for analysis are screened and improved from the viewpoint of design restriction. Without correction, the analysis of unqualified cases causes a waste of computing power and time by considering inaccurate results or analysis failure.

One of the design restrictions we faced during the CIPT design was relative physical limitation violation. According to the practical winding method, we assumed the coil area always attaches to the lower-middle corner, which is the lower-right corner in the left-half model. So, the relative limitation can be seen to be that the lateral and horizontal lengths of the coil are not allowed to exceed the corresponding inner edges of the core, as shown in the left-half model in Figure 8, where two blue U shapes stand for the maximum and minimum core area, and the other two red rectangles give the maximum and minimum coil areas. The relative physical limitation might be violated in the marked overlap area between core and coil. If such an area exists in a candidate, it should be considered to be unavailable as it is not capable of generating valid results. As for the I-shaped core, the correction procedure only examines the lateral edges.

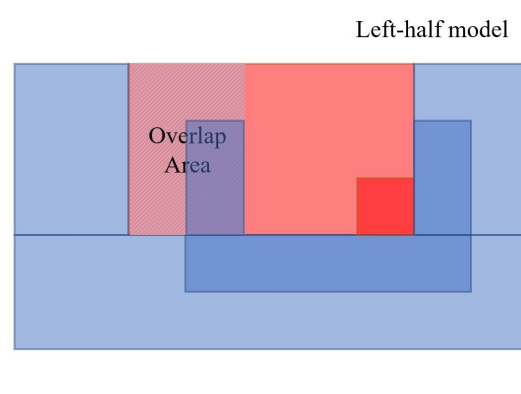


**Figure 8.** Example of the overlap area.

In practical applications, we need to consider the relation to other components, such as car bodies and ground facilities. This often creates complicated restrictions for the size and shape of the external cross-section. However, it is straightforward to consider such restrictions in the process of violation detection and correction.

Auto resistance calculation is applied to give the proximate resistance of the coil when the corresponding checkbox is checked in the interface. Due to the characteristic of the E-like core, the coil is assumed to be wound around the central pole or an imaging block. The cross-sectional area and length of the coil are calculated based on the user-defined parameters; then the software considers the coil area is filled with mechanically shaped Litz wire, since Litz wire is popular for high-frequency applications due to its ability to diminish skin proximate effects. The mechanically shaped wire enables optimal utilization of the available winding space due to the superior filling factor of rectangular or square Litz wire cross-sections. First, the strand specifications are determined out of the America MW1000C gauge according to the skin depth which is given as

$$\delta = \sqrt{\frac{\rho}{\pi f \mu_0}} \quad (1)$$

where  $\rho$  is the resistivity of the conductor,  $f$  is the frequency, and  $\mu_0$  is the permeability of free space. Based on [25], the AC resistance can be approximately acquired using the AC resistance factor as

$$k = \frac{R_{AC}}{R_{DC}} = 1 + \frac{(\pi n N)^2 d_s^6}{192 \times \delta^4 \times b^2} \quad (2)$$

where  $n$  is the strand amount,  $N$  is the turns,  $d_s$  is the strand diameter, and  $b$  is the coil breadth, which is the coil width in this case. Then the DC resistance of the coil is given as

$$R_{DC} = (1 + \sum_1^{n_b} 0.02) \times \frac{N R_{sDC}}{n} \quad (3)$$

where  $n_b$  is the bunching factor and  $R_{sDC}$  is the resistance of the single strand. By multiplying (2) and (3), the coil resistance under a certain frequency is acquirable. No matter which approach is involved, the auto resistance calculation can be applied every time before the FEM analysis.

As they are the fundamental elements of a geometric figure, the vertices are used to build the geometry instead of the edges. The drawing method of locating and connecting the vertices can ensure the graphics' accuracy and be recognized by most drawing tools, significantly increasing the software's compatibility with the FEM solver. On the other hand, it is easier for the user to define the parameters, and less complicated for optimal analysis, to produce springs by use of the edges instead of the vertices for the lower quantity. So, parameter transformation is placed in the middle of the candidates handled and the FEM process provides convenience for both ends. As shown in the example of an EE-shaped structure in Figure 2, the transformation section defines one vertex as the origin

(the red dot), and derives the coordinates of the other vertices (the blue dots) from the edge information. The vertices data is then passed to the next step.

### 2.2.2. Analysis Status Control

Procedures such as script generation, FEM analysis, and compensation calculation are considered under the analysis status control block. Commanding, running, monitoring, and summarizing are the main functions of this block.

Before every set of analyses, the software creates the analysis scripts according to the customized parameters and feedback from previous steps. There are two types of analysis sets arranged in series when obtaining a comprehensive evaluation of a CIPT device: inductance measurement and compensation performance. The induction measurement is to measure the self and mutual inductance of the primary and secondary coils. The compensation performance is to test the effects of the selected compensation topology and capacitance provided by the software. The script generation block prepares a bunch of snippets corresponding to the different behaviors of the FEM analysis so that customized analysis can be accomplished that satisfies the different analysis requirements by combining the script snippets in various orders.

In the proposed software, we use third-party FEM solvers instead of providing one. When the FEM analysis section is called for the first time, the software will launch the FEM solver specified by the user. The whole FEM analysis is under the control of the generated scripts and the software. After the analysis is launched by the script, the software applies a real-time monitor ensuring uninterrupted running. As shown in Table 1, the current state of the analysis process can be confirmed according to the analysis window's existence, the list of files in the results folder, and the modified state of the folder. To achieve efficient automatic operation, the software monitors the status in real-time and triggers the following process for the save completed state. Monitoring of the analysis window is the first layer of monitoring. It avoids frequent accessing of the same address. In the second layer, the folder modified state monitoring distinguishes the analysis interval from the analysis end. The file list checks if the saving process finishes or not. The whole second layer is responsible for securing the effectiveness of monitoring in case of failing to detect the saving file state (assuming that the temporary file appears extremely short at the end of the compensation analysis). This method ensures high speed and accuracy while avoiding the need to communicate with third-party software. The versatility of this block is enhanced while reducing complexity.

**Table 1.** Analysis process state.

Analysis State	Analysis Window Existence	File State	Folder Renewal
Initialization	No	+project files	Yes (create)
Script loading	No	Same as previous	No
Analysis in progress	Yes	Same as previous	No
Analysis gap	No	Same as previous	No
Saving data	No	+temporary files	Yes
Saved	No	−temporary files +results files	Yes

An open-short circuit test is executed to acquire the self and mutual inductance in inductance measurement analysis. The self-inductance is calculated by (4) when the secondary and primary are open, respectively, and the coil resistance is ignored.

$$L_{1,2} = \frac{Re(I_{1,2}) \times Im(V_{1,2}) - Re(V_{1,2}) \times Im(I_{1,2})}{2\pi f} \quad (4)$$

where  $L_1$  is the self-inductance calculated using the real and imaginary part of the voltage and current as  $Re(V_1)$ ,  $Re(I_1)$ ,  $Im(V_1)$  and  $Im(I_1)$  when the primary side is connected to the power source and the secondary side is open. Similarly, the self-inductance of the

secondary side  $L_2$  is given by the real and imaginary part of the voltage and current of the secondary side  $Re(V_2)$ ,  $Re(I_2)$ ,  $Im(V_2)$  and  $Im(I_2)$  when the primary side is open-circuit.

The short circuit test is for calculating the leakage inductance as

$$L_{l1,l2} = \frac{Re(I_{l1,l2}) \times Im(V_{l1,l2}) - Re(V_{l1,l2}) \times Im(I_{l1,l2})}{2\pi f} \quad (5)$$

where  $L_{l1}$ ,  $L_{l2}$  is the leakage inductance of the primary and secondary sides and  $Re(V_{l1})$ ,  $Re(I_{l1})$ ,  $Im(V_{l1})$ ,  $Im(I_{l1})$ ,  $Re(V_2)$ ,  $Re(I_2)$ ,  $Im(V_2)$  and  $Im(I_2)$  are the real and imaginary currents and voltages of the primary and the secondary side, respectively, when the opposite side is shorted.

Then the mutual inductance is obtainable as

$$M = L_1 - L_{l1} = L_2 - L_{l2} \quad (6)$$

The software can give the capacitance for compensation based on the selected topology and the results of inductance measurement. After applying the induction measurement, if required, the compensation performance can be automatically applied using the calculated capacitance. The secondary capacitance is used to adjust the secondary resonant frequency to the same value of the frequency of the power source given by

$$C_2 = \frac{1}{\omega^2 L_2} \quad (7)$$

where  $C_2$  stands for the secondary capacitance and the  $\omega = 2\pi f$  is the resonant frequency. The primary compensation is assumed to absorb the remaining reactive power. Its value is different according to the topology.

$$C_{1ss} = \frac{1}{\omega^2 L_1} \quad (8)$$

$$C_{1sp} = \frac{1}{\omega^2 (L_1 - \frac{M^2}{L_2})} \quad (9)$$

$$c_{1ps} = \frac{L_1}{\left\{ \frac{(\omega M)^2}{R} \right\}^2 + (\omega L_1)^2} \quad (10)$$

$$c_{1pp} = \frac{L_1 - \frac{M^2}{L_2}}{\left( \frac{M^2 R}{L_2^2} \right)^2 + \omega^2 (L_1 - \frac{M^2}{L_2})^2} \quad (11)$$

### 2.2.3. Grid Analysis

The grid mode sets a group of analysis cases that the target parameters increase gradually by a certain interval. It provides a complete image of performance on the design space considering the intervals of the parameter changes as the accuracy. The influence of different parameters on the performance, whether this is a one-to-one, one-to-many, or many-to-many correspondence, can be observed easily in a one-time setting. The geometry and circuit parameters are available in this mode, as shown in Figure 5a. As the flowchart indicates in Figure 7, the grid mode creates a matrix of the target parameters from the minimum value to the maximum value at once. Then, in the data correction step, all the candidates in the matrix are examined, and those that have overlapping areas are removed from the grid design space so that no computing power is wasted. The remaining candidates take part in the upcoming steps until the end. In this analysis mode, all the procedures are performed only once, so hardly any valuable data is retained if the analysis stops in the middle; however, the chance of being interrupted by mis-operation or another program is lower.

#### 2.2.4. Optimal Analysis

The optimal analysis mode uses a modified NSGA-II method which searches for the optimal solution that matches the desired objectives in a given design space, regardless of whether the trend in the space is known or not. If it exists, the optimal solution should be located using fewer cases of analysis compared to the grid analysis mode; however, it is much less possible to indicate the relationship between the design parameters and performance. The flow of the optimal analysis mode is as shown in Figure 7.

The customizable parameters and objectives are as shown in Figure 5b. An arbitrary number of parameters and objectives can be selected by checking the checkbox in front of each of them, though at least one parameter and one objective are necessary as minimal requirements to start the optimization process. For the parameters, the upper limit is set in the optimization block of the graphic interface, while the lower limit is taken from the input in other blocks. For the objectives, the output power, efficiency, coupling coefficient, output voltage, and output current are provided and defined. The output power, efficiency, and coupling coefficient are considered as maximum optimal problems; the output voltage and output current are considered to be middle-value optimal problems. The objectives are then converted to the universal value set that can be processed as minimal problems. Therefore, the fitness of the solution is the distance between it and the optimal point. The fitness definition for each objective in its general form is given by:

$$\begin{aligned}
 \text{Fit}_m(X) &= \begin{cases} f_{m_{\max}} - f_m(X), & \text{for maximum problem} \\ \left| \frac{f_{m_{\min}} + f_{m_{\max}}}{2} - f_m(X) \right|, & \text{for middle-value problem} \end{cases} \quad m = 1, 2, \dots, M \\
 \text{s.t. } g_{m_{\text{lower}}}(X) &= f_m(X) - f_{m_{\min}} \geq 0, \\
 g_{m_{\text{upper}}}(X) &= f_m(X) - f_{m_{\max}} \leq 0, \\
 x_{n_{\min}} &\leq x_n \leq x_{n_{\max}}. \quad n = 1, 2, \dots, N
 \end{aligned} \tag{12}$$

where the  $X = [x_1, x_2, \dots, x_N]$  is the set of parameters with  $N$  variables,  $x_{n_{\min}}$  and  $x_{n_{\max}}$  are the constraints for the parameter  $n$ . The  $f_m(X)$  is the  $m$  in  $M$  objectives in the solution composed by  $X$ .

The randomly generated first generation is examined in the data correction section. A physical restraint violation is foreseeable in the population generation process since the GA does not consider the original practical conditions. So, every generation is examined directly before the analysis. Rather than take out the candidates, as in the grid analysis mode, in the optimal analysis mode, if any violation is detected, the distal edge of the exceeded part is forced to be the maximum possible position corresponding to the relevant part, since a smaller size is generally desirable.

A complete offspring generation consists of selection, crossover, and mutation. This software adopts the NSGA-II method proposed by [26]. The NSGA-II performs a fast, non-dominated, sorting that increases the probability of individuals with more information being sorted to the next generation as the selection. Since the FEM analysis is generally time-consuming, the concept of GA parameter setting in our software is to maintain the capacity for convergence within a small number of individuals and still reach out to other areas in the design space and escape from the local optimal. There are a few methods that can be used for the GA parameter setting, such as [27]. However, it is hard to find a set of GA parameters for problems with constantly changing design spaces and objective ranges. So, we set the parameters such that the optimal process retains a high possibility of evolution, distributed within a medium range compared with the design space. It should be noted that the setting is not verified in all of the scenarios, but provides an acceptable variable distribution in our tests and example. Our software applies the simulated binary crossover as the crossover method. In the crossover operator, we set the probability of crossover as 0.9, as the parents have a 90% chance of crossover. The distribution index has a direct effect on controlling the spread of the offspring—the bigger value gives a higher probability of creating solutions similar to the parents. We set it equal to three, under which value

the crossover operator tends to perform middle-scale offspring generation. The mutation operator uses polynomial mutation. The probability of mutation is  $\frac{1}{\text{number of variables}}$  and the distribution index is three for the same reason as in the crossover.

The optimization process finishes under two statuses: reaching the maximum generation or meeting the termination condition. A termination condition is set to finish the process in advance if the solution set accumulates in the optimal area. In this software, a termination considers the design space tolerance to shorten the time consumption if possible. The design space tolerance compares the parameters of the current solutions and those of historical solutions. If the difference is below the tolerance, the process will terminate. A cycle, instead of every generation, is usually set to evaluate the objective space to reduce the computational intensity. To avoid extreme solutions triggering the termination condition, it is usually stipulated that the evaluation starts after a certain number of generations. Since the user of the software defines the total number of generations, a corresponding termination criterion is required to ensure the regular operation of the terminator. The authors set the tolerance to 0.005, the evaluation interval as one-tenth of the entire generations (force to 1 if less than 1), and the starting position of the evaluation to one-third of the generation number (force to 1 if less than 1).

### 2.3. Post-Analysis Process

The post-analysis section is responsible for results collection and converting the analysis results to a read-friendly form. Tables and figures are available as means of displaying results. Other than the original data, a table of coupling coefficients is provided when compensation is not applied, and the table carries comprehensive output performance and design details. In optimal analysis mode, the Pareto front, which is the set of non-dominated solutions, being chosen as optimal so that no objective can be improved without deducing at least one other objective, is collected in an exclusive table for the user to quickly check. All the data is arranged in the order of execution so that the user can easily trace back to any specific case. In both analyses, the parallel coordinate plot (PCP) and N-dimensional scatter are available. The grid analysis mode provides the PCP of the altered parameters and the outputs. For analysis, where three or more parameters are involved, the scatter will not be drawn since it indicates less observable information. When there is only one parameter, a group of 2D scatters is generated showing the parameter-output relationship for every output item. Similarly, the results for two parameters come with 3D scatters. The optimal analysis mode shows the analyzed cases with the chosen parameters and objectives in the PCP that delivers the accumulated results. We apply the PCP that produces an HTML file that features an exchangeable axis and highlight axis range so that the preferred solution can be easily found, or shifts observed in the design space. An N-dimensional (N equals the number of selected objectives) scatter figure shows the Pareto front, presenting the performance of the most optimized solutions. Finally, all related progress is shut down with a confirmation message of analysis complete.

### 3. Examples

Two examples are presented in this paper to demonstrate the grid analysis mode and the optimal analysis mode of the proposed software, respectively. To demonstrate the fundamental novelty of our proposal, we do not consider any complicated external conditions, so as to avoid particular characteristics that are not easy to generalize. The JMAG as the FEM solver, and the Ploty as part of the figuring engine for the results display, are used in solving these examples. No manual operation occurs after parameter definition in both examples until the end. These examples run on a machine with four cores without GPU acceleration using the i5-6400 CPU with 16 GB RAM. The total time for the examples is given but please note that the analysis time depends on the machine configuration and cases generated.

### 3.1. Example of Grid Analysis

The parameters of this example are shown in Table 2. The width of the coil area and the distance of the core poles are selected as the parameters vary independently from 50 mm to 200 mm. Originally, there were  $(\frac{200-50}{10} + 1)^2 = 256$  cases for the parameter range and interval but  $(1 + 16) \times \frac{16}{2} = 136$  cases were submitted for analysis after data correction. This process took around three hours to complete.

Since there are only two parameters selected as the grid elements, the 3D scatters for each output are created as illustrated above in Figure 9. It can be seen that the coupling coefficient and efficiency follow the increments of the coil and core; however, the output voltage, current, and power tend to drop in the middle. As in this example, sometimes the scatter fails to give a clear image of the distribution, then the PCP gives a better impression of the performance. Figure 10 demonstrates the solutions in PCP; Figure 10a presents the distribution of design space and outputs indicating the higher output power appears at a larger pole distance with an intermediate coil area width. Figure 10b, highlighting the solutions where the pole distance is 200 mm, provides a local set for further investigation.

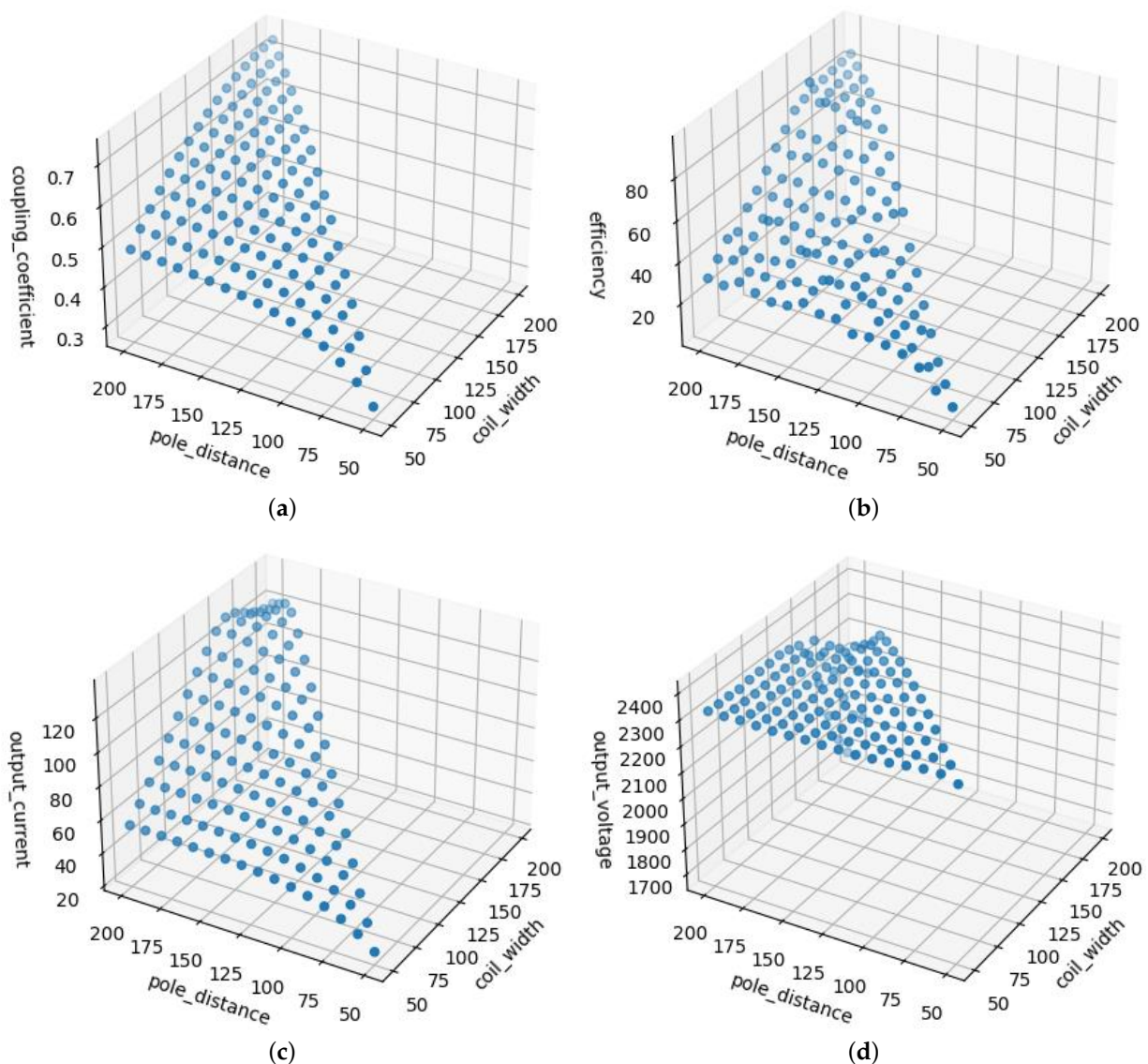
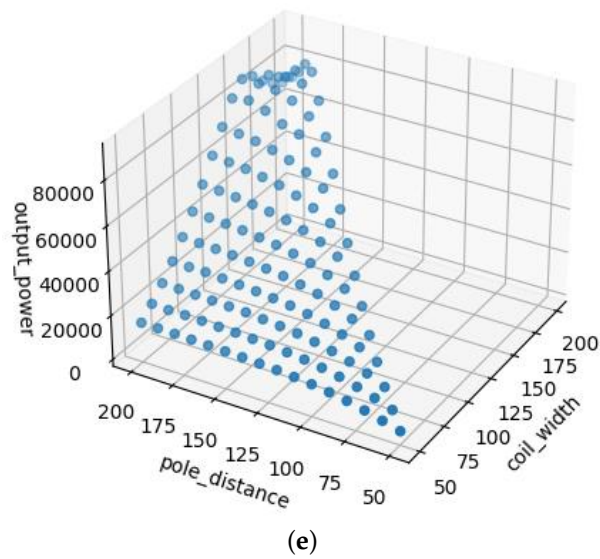
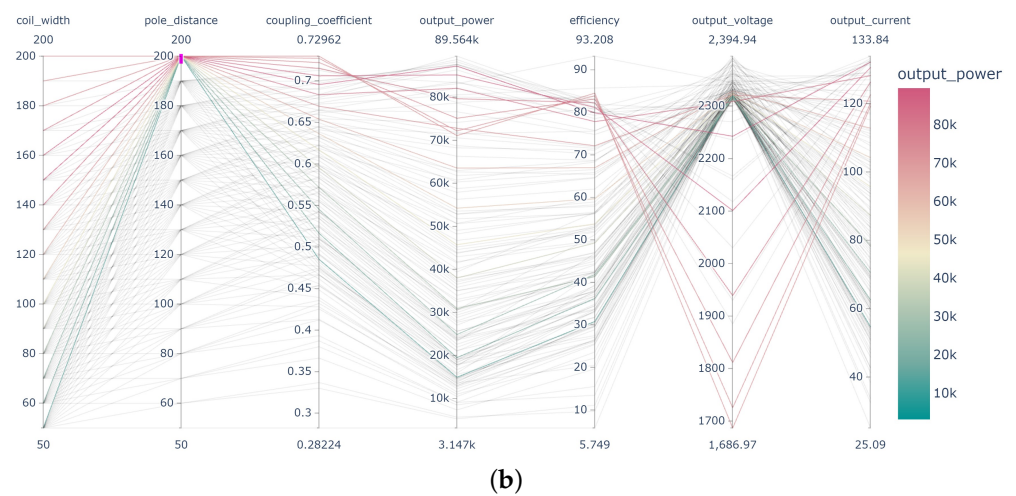
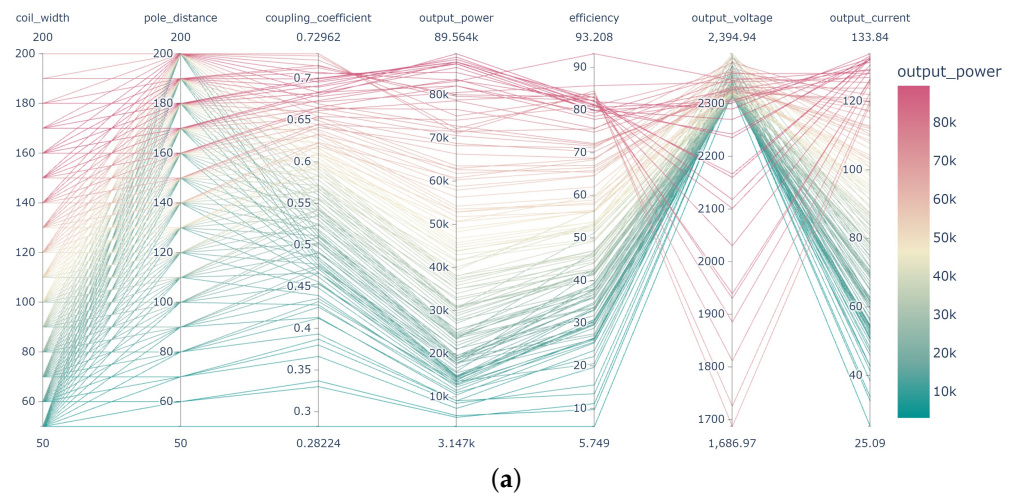


Figure 9. Cont.



**Figure 9.** Scatters of grid analysis example. They show the relation amount parameters with (a) coupling coefficient, (b) efficiency, (c) output current, (d) output voltage, and (e) output power.



**Figure 10.** PCP of grid analysis example as (a) overall display and (b) highlight display.

**Table 2.** The setting of grid analysis mode example.

Coil	Width (min/interval/max)		50/10/200 mm
	Height		45 mm
	Turns	Primary	2
		Secondary	50
	Resistance		Auto
Material		Copper	
Core	Shape		EE without legs
	Pole	Height	45 mm
		Thickness	20 mm
		Distance (min/interval/max)	50/10/200 mm
	Base Thickness		10 mm
	Depth		1000 mm
Initial Relative Permeability		2300	
Air gap		50 mm	
Power source	Type		Current
	Amplitude		100 A
Compensation Type		PP	
Load		10 $\Omega$	
Mesh	Entity		3 mm
	Air		5 mm
Number of cases		136 out of 256	

### 3.2. Example of Optimal Analysis

In this example, we demonstrate the automatic optimization process with a set of given parameters, assuming the device is developed for high-power applications, such as EVs or trains, that have vertical and lateral extension limitations [28,29]. The detailed design parameters are showing as in Table 3. Two hundred cases are progressed in this example; the whole process took around 9 h without manual intervention.

The software gathers the data as a Pareto front and overall information in the form of tables and figures. A three-dimensional scatter of the Pareto front as Figure 11 is given in this example according to the number of objectives. It introduces the performance of the optimal set. The specific parameters and outputs are summarized in Table 4; the magnetic field distribution at 30 degree is given in Figure 12. The same materials are available in the results folder for further research. The user can select the design that matches the requirement; for example, case 193 holds the output voltage closest to 1500 V as the desired value with fine output power and ideal efficiency. However, situations where the process fails to find the Pareto front within limited generations, or suitable individuals appear outside the Pareto front, could occur. The PCP provides help finding the acceptable design from all individuals or enables adjusting of the parameter range for the coming analysis. As the PCP of example 2 demonstrates, the accumulation of parameters during the process, as in Figure 13a, and, by selecting the range of axes, the user can check that the solutions were in the objective range, as in Figure 13b, and search for the solutions that best meet the requirements. Showing the entire results, instead of the Pareto front, as PCP means transferring the optimal selection to the user, since the optimal Pareto front might not fulfil the practical demand.

**Table 3.** The setting of optimal analysis mode example.

Design Space			
Coil	Width		50~200 mm
	Height		45~60 mm
	Turns	Primary	1~10
		Secondary	1~50
	Resistance		Auto
Material		Copper	
Core	Shape		EE with legs
	Pole	Height	45~60 mm
		Thickness	20~50 mm
		Distance	50~200 mm
	Leg	Length	100 mm
		Thickness	14 mm
	Base Thickness		10 mm
	Depth		1000 mm
Initial Relative Permeability		2300	
Air gap		50 mm	
Power source	Type	Current	
	Amplitude	100 A	
Compensation Type		SS	
Load		10~50 Ω	
FEM Settings			
Mesh	Entity		3 mm
	Air		5 mm
GA Settings			
Population Size		10	
Generation		20	
Algorithm		NSGA-II	
Crossover	Method	Simulated Binary Crossover	
	Probability	0.9	
	Distribution Index	3	
Mutation	Method	Polynomial Mutation	
	Probability	$\frac{1}{N_{variables}} = 0.125$	
	Distribution Index	3	
Objectives			
Output Power (maximum optimal)		20,000~100,000 W	
Efficiency (maximum optimal)		70~100%	
Output Voltage (median optimal)		1350~1650 V	

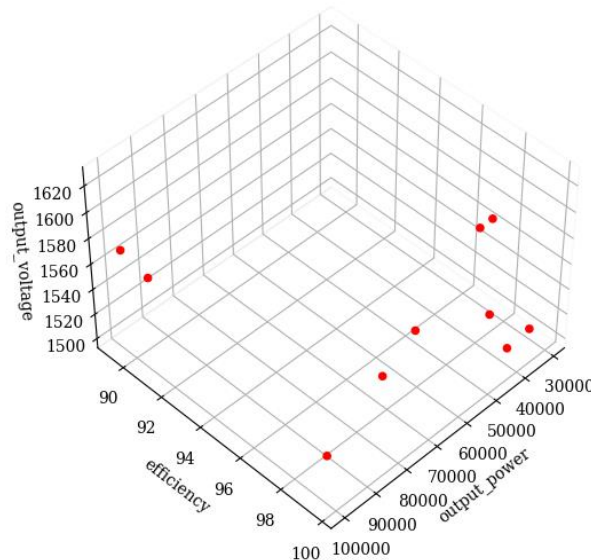


**Figure 11.** Pareto front of the optimal analysis example.

**Table 4.** The parameters of the generated Pareto front.

Case	$P_{out}$ (W)	$\eta$ (%)	$U_{out}$ (V)	Coil Width (mm)	Coil Height (mm)	Pole Distance (mm)	Pole Thickness (mm)	Pole Height (mm)	Primary Coil Turns	Secondary Coil Turns	Load ( $\Omega$ )	Primary Resistance ( $\Omega$ )	Secondary Resistance ( $\Omega$ )
130	99,413.98	89.39	1570.97	117	45	117	42	45	3	25	10.27	$2.90 \times 10^{-3}$	$2.01 \times 10^{-1}$
193	92,188.65	98.39	1501.23	116	45	116	26	45	3	25	12.18	$2.85 \times 10^{-3}$	$1.98 \times 10^{-1}$
166	31,178.27	99.37	1504.36	115	45	116	24	50	3	26	36.29	$2.86 \times 10^{-3}$	$2.15 \times 10^{-1}$
196	49,060.29	99.67	1625.02	115	45	115	24	50	7	12	26.91	$1.56 \times 10^{-2}$	$4.58 \times 10^{-2}$
182	98,504.79	90.61	1561.58	117	45	117	44	45	3	25	10.50	$2.91 \times 10^{-3}$	$2.02 \times 10^{-1}$
200	44,813.74	99.22	1538.66	116	45	116	27	50	3	25	26.41	$2.85 \times 10^{-3}$	$1.98 \times 10^{-1}$
114	66,356.95	98.74	1558.62	116	45	116	24	50	3	25	15.65	$2.84 \times 10^{-3}$	$1.97 \times 10^{-1}$
183	53,120.27	99.67	1624.95	115	45	115	24	50	7	12	24.85	$1.56 \times 10^{-2}$	$4.58 \times 10^{-2}$
141	41,328.28	99.67	1510.37	115	45	115	24	50	7	11	26.85	$1.56 \times 10^{-2}$	$3.85 \times 10^{-2}$
180	82,375.22	99.53	1561.52	95	45	114	24	54	7	11	12.56	$1.84 \times 10^{-2}$	$4.54 \times 10^{-2}$

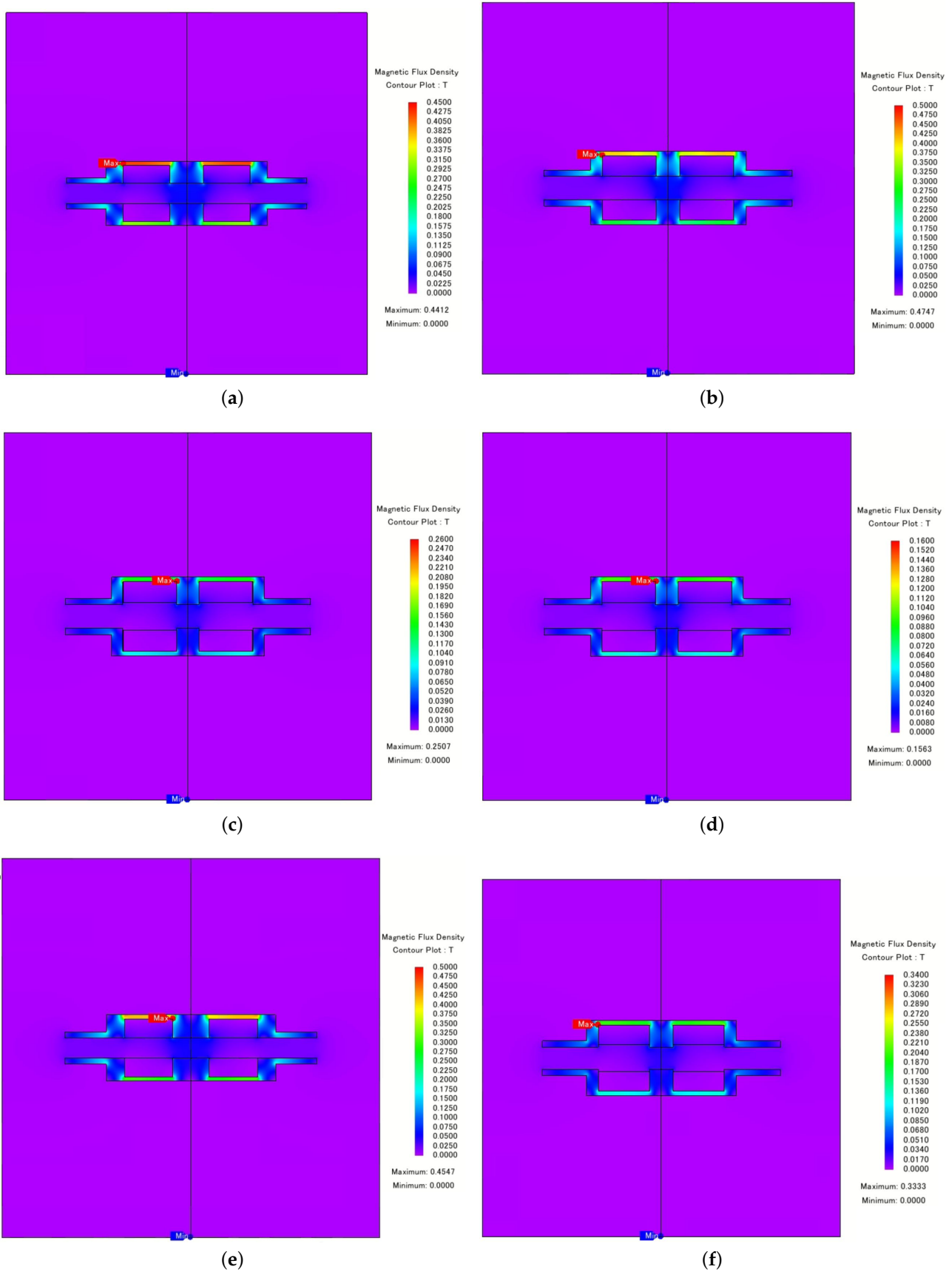
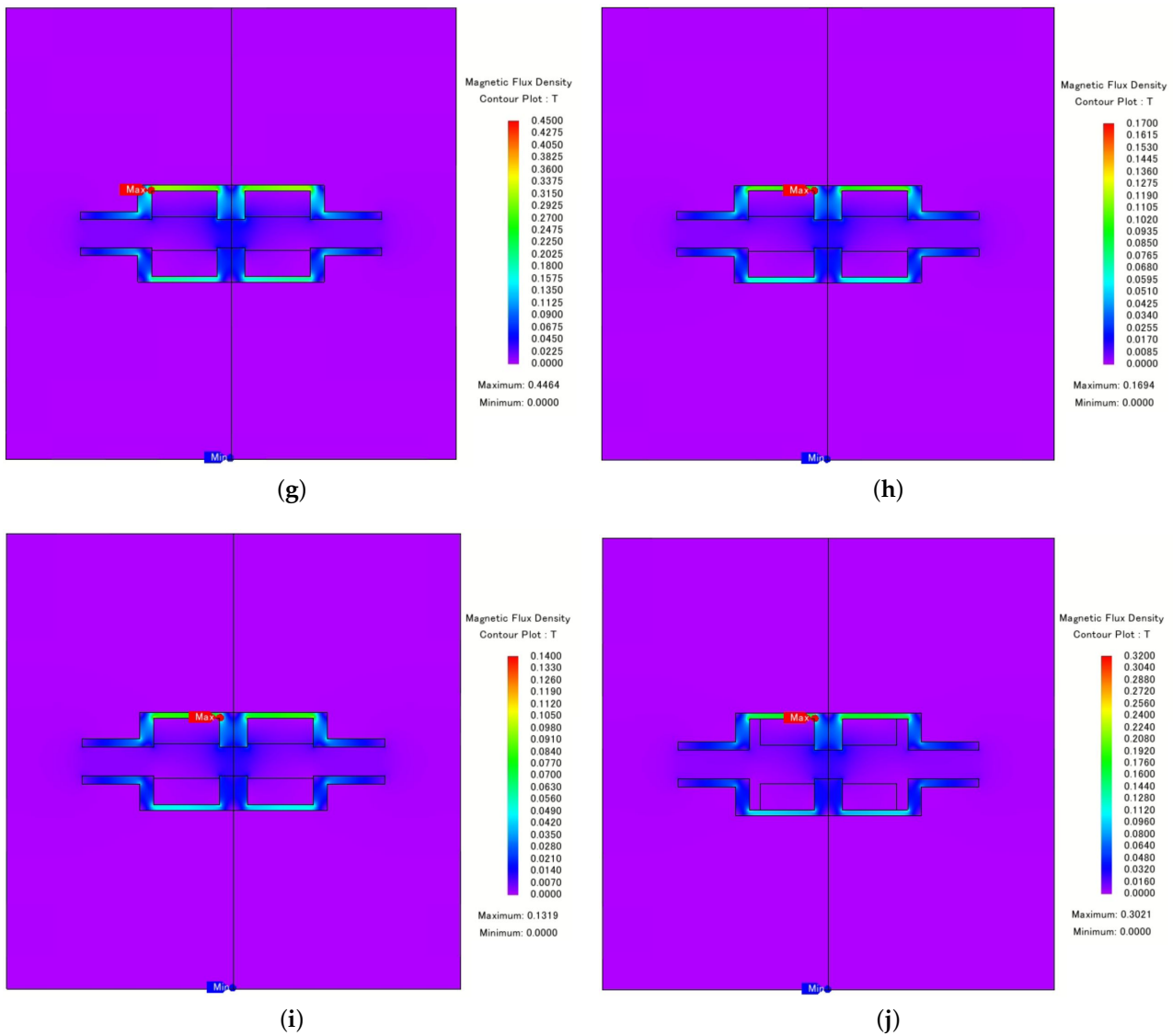
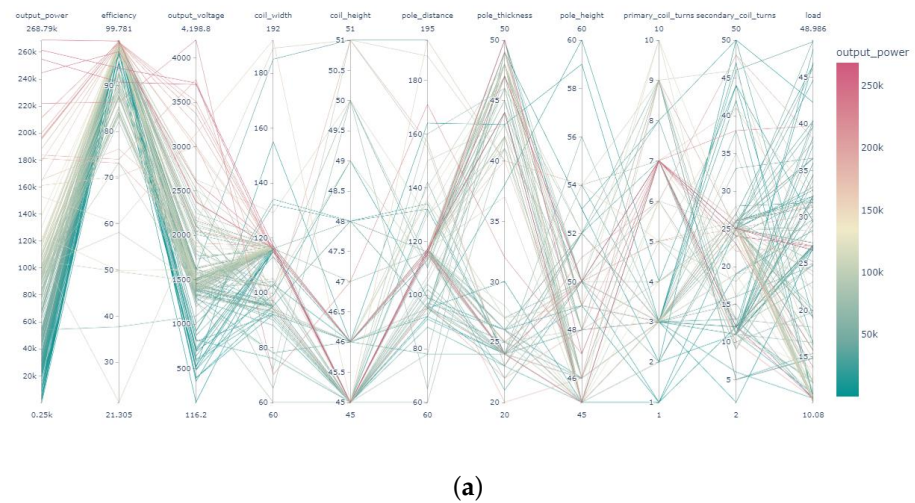


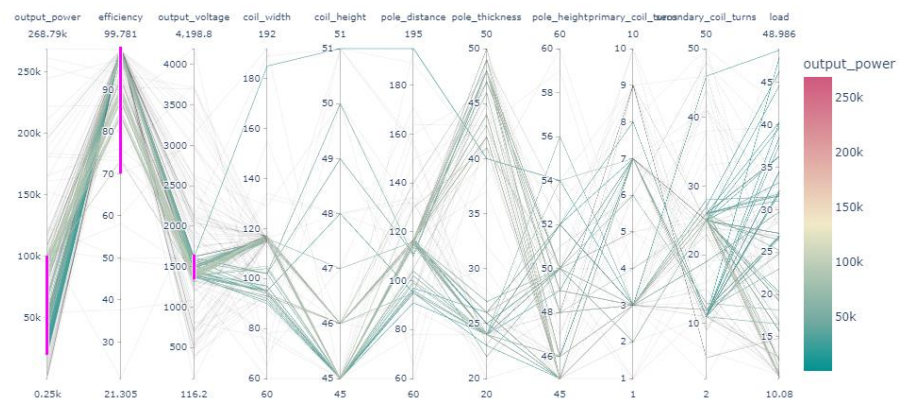
Figure 12. Cont.



**Figure 12.** The Pareto front of example 2 at (a) case 130, (b) case 193, (c) case 166, (d) case 196, (e) case 182, (f) case 200, (g) case 114, (h) case 183, (i) case 141, and (j) case 180.



**Figure 13.** Cont.



(b)

**Figure 13.** PCP of optimal analysis example as (a) overall display and (b) highlight display.

#### 4. Conclusions

This paper introduces a software tool for CIPT design that improves the flexibility and productivity of CIPT design by collaborating with the JMAG as the FEM solver and the Plotly as part of the figuring engine for the results display. Compared with manual operation, it dramatically reduces requirements for user familiarity and proficiency with the FEM solver by providing an integrated and simplified interface. It also offers automatic operation that frees the user from tedious and repetitive work. The automation includes solution generation in different analysis modes, analysis building, simulation status detection, compensation calculation, data correction, resistance calculation, and results display.

A grid analysis mode and optimal analysis mode are built into the software. The grid analysis mode allows the user to define variable limitations and intervals and then feeds back the performance of every effective solution. The optimal analysis mode uses the NSGA-II algorithm to search for the optimal solution in the user-defined design space. Adjusting the variables, generation, population, and objectives is achievable by use of the correction function. Two examples are given to demonstrate the approaches, and to illustrate the capabilities of the automatic process. It is noticeable that less than twice the cases require four times the time for optimal analysis compared with grid analysis in our examples. This occurs since the FEM analysis needs to load the parameters every generation in optimal analysis but only once in grid analysis. However, the accuracy in the local optimal design area is higher for optimal analysis than for grid analysis. Moreover, when more and more variables are involved in the analysis, the number of solutions increases dramatically, when the optimal analysis might manage to present the optimal solutions with a relatively small number of solutions. The selection of the analysis mode should be undertaken on a case-by-case basis, with potentially improved solutions by their combination.

**Author Contributions:** Conceptualization, Y.L.; methodology, Y.L.; software, Y.L.; validation, Y.L. and M.M.; formal analysis, Y.L.; investigation, Y.L.; resources, Y.L. and M.M.; data curation, Y.L.; writing—original draft preparation, Y.L.; writing—review and editing, M.M.; visualization, Y.L.; supervision, M.M.; project administration, Y.L.; funding acquisition, M.M. All authors have read and agreed to the published version of the manuscript.

**Funding:** This research received no external funding.

**Institutional Review Board Statement:** Not applicable.

**Informed Consent Statement:** Not applicable.

**Data Availability Statement:** Not applicable.

**Acknowledgments:** The authors would like to thank all the colleagues in Miyatake's laboratory for their kindly help.

**Conflicts of Interest:** The authors declare no conflict of interest.

## References

1. Lee, S.H. Design Methodologies for Low Flux Density, High Efficiency, kW Level Wireless Power Transfer Systems with Large Air Gaps. Ph.D. Thesis, University of Wisconsin-Madison, Madison, WI, USA, 2013.
2. Campi, T.; Cruciani, S.; Maradei, F.; Feliziani, M. Two-Coil Receiver for Electrical Vehicles in Dynamic Wireless Power Transfer. *Energies* **2021**, *14*, 7790. [[CrossRef](#)]
3. Liu, C.Y.; Wang, G.B.; Wu, C.C.; Chang, E.; Cheng, S.; Chieng, W.H. Derivation of the Resonance Mechanism for Wireless Power Transfer Using Class-E Amplifier. *Energies* **2021**, *14*, 632. [[CrossRef](#)]
4. Lu, F.; Zhang, H.; Mi, C. A Review on the Recent Development of Capacitive Wireless Power Transfer Technology. *Energies* **2017**, *10*, 1752. [[CrossRef](#)]
5. Kim, J.; Kim, D.H.; Kim, J.; Park, Y.J. Wireless Power Transfer between Two Self-Resonant Coils over Medium Distance Supporting Optimal Impedance Matching Using Ferrite Core Transformers. *Energies* **2021**, *14*, 8540. [[CrossRef](#)]
6. Fujita, T.; Yasuda, T.; Akagi, H. A Dynamic Wireless Power Transfer System Applicable to a Stationary System. *IEEE Trans. Ind. Appl.* **2017**, *53*, 3748–3757. [[CrossRef](#)]
7. Lee, S.; Jung, G.; Shin, S.; Kim, Y.; Song, B.; Shin, J.; Cho, D. The optimal design of high-powered power supply modules for wireless power transferred train. In Proceedings of the 2012 Electrical Systems for Aircraft, Railway and Ship Propulsion, Bologna, Italy, 16–18 October 2012; IEEE: Bologna, Italy, 2012; pp. 1–4. [[CrossRef](#)]
8. Zaheer, A.; Covic, G.A.; Kacprzak, D. A Bipolar Pad in a 10-kHz 300-W Distributed IPT System for AGV Applications. *IEEE Trans. Ind. Electron.* **2014**, *61*, 3288–3301. [[CrossRef](#)]
9. Lee, D.S.; Jang, D.U.; Kim, H.C.; Jung, S.Y. Numerical Analysis and Design of Moving Contactless High Power Transformer. *J. Magn.* **2011**, *16*, 423–426. [[CrossRef](#)]
10. Huh, J.; Lee, S.W.; Lee, W.Y.; Cho, G.H.; Rim, C.T. Narrow-Width Inductive Power Transfer System for Online Electrical Vehicles. *IEEE Trans. Power Electron.* **2011**, *26*, 3666–3679. [[CrossRef](#)]
11. Shin, J.; Shin, S.; Kim, Y.; Ahn, S.; Lee, S.; Jung, G.; Jeon, S.J.; Cho, D.H. Design and Implementation of Shaped Magnetic-Resonance-Based Wireless Power Transfer System for Roadway-Powered Moving Electric Vehicles. *IEEE Trans. Ind. Electron.* **2014**, *61*, 1179–1192. [[CrossRef](#)]
12. Zhang, W.; Chen, Q.; Wong, S.; Tse, C.; Ruan, X. A novel transformer for contactless energy transmission systems. In Proceedings of the 2009 IEEE Energy Conversion Congress and Exposition, San Jose, CA, USA, 20–24 September 2009; IEEE: San Jose, CA, USA, 2009; pp. 3218–3224. [[CrossRef](#)]
13. Liu, F.; Yang, Y.; Jiang, D.; Ruan, X.; Chen, X. Modeling and Optimization of Magnetically Coupled Resonant Wireless Power Transfer System with Varying Spatial Scales. *IEEE Trans. Power Electron.* **2017**, *32*, 3240–3250. [[CrossRef](#)]
14. Aydin, E.; Aydemir, M.T.; Aksoz, A.; El Baghdadi, M.; Hegazy, O. Inductive Power Transfer for Electric Vehicle Charging Applications: A Comprehensive Review. *Energies* **2022**, *15*, 4962. [[CrossRef](#)]
15. Bagheri, A.; Erfanian, A.; Abrishamifar, A. A Systematic Methodology for Optimal Design of Wireless Power Transfer System Using Genetic Algorithm. *Energies* **2020**, *13*, 383. [[CrossRef](#)]
16. Bertoluzzo, M.; Giacomuzzi, S.; Sieni, E. Automatic Optimization of the Compensation Networks of a Wireless Power Transfer System. *Energies* **2020**, *13*, 5298. [[CrossRef](#)]
17. Shimode, D.; Murai, T.; Fujiwara, S. A Study of Structure of Inductive Power Transfer Coil for Railway Vehicles. *IEEJ J. Ind. Appl.* **2015**, *4*, 550–558. [[CrossRef](#)]
18. Stielau, O.; Covic, G. Design of loosely coupled inductive power transfer systems. In Proceedings of the PowerCon 2000, 2000 International Conference on Power System Technology, Proceedings (Cat. No.00EX409), Perth, WA, Australia, 4–7 December 2000; IEEE: Perth, WA, Australia, 2000; Volume 1, pp. 85–90. [[CrossRef](#)]
19. Wang, C.S.; Covic, G.; Stielau, O. Power Transfer Capability and Bifurcation Phenomena of Loosely Coupled Inductive Power Transfer Systems. *IEEE Trans. Ind. Electron.* **2004**, *51*, 148–157. [[CrossRef](#)]
20. Sohn, Y.H.; Choi, B.H.; Lee, E.S.; Lim, G.C.; Cho, G.H.; Rim, C.T. General Unified Analyses of Two-Capacitor Inductive Power Transfer Systems: Equivalence of Current-Source SS and SP Compensations. *IEEE Trans. Power Electron.* **2015**, *30*, 6030–6045. [[CrossRef](#)]
21. Aditya, K.; Williamson, S.S. Comparative study of Series-Series and Series-Parallel compensation topologies for electric vehicle charging. In Proceedings of the 2014 IEEE 23rd International Symposium on Industrial Electronics (ISIE), Istanbul, Turkey, 1–4 June 2014; IEEE: Istanbul, Turkey, 2014; pp. 426–430. [[CrossRef](#)]
22. Hao Hao.; Covic, G.A.; Boys, J.T. A Parallel Topology for Inductive Power Transfer Power Supplies. *IEEE Trans. Power Electron.* **2014**, *29*, 1140–1151. [[CrossRef](#)]
23. Zhang, W.; Wong, S.C.; Tse, C.K.; Chen, Q. Analysis and Comparison of Secondary Series- and Parallel-Compensated Inductive Power Transfer Systems Operating for Optimal Efficiency and Load-Independent Voltage-Transfer Ratio. *IEEE Trans. Power Electron.* **2014**, *29*, 2979–2990. [[CrossRef](#)]

24. Wang, C.S.; Stielau, O.; Covic, G. Design Considerations for a Contactless Electric Vehicle Battery Charger. *IEEE Trans. Ind. Electron.* **2005**, *52*, 1308–1314. [[CrossRef](#)]
25. Sullivan, C.R.; Zhang, R.Y. Simplified design method for litz wire. In Proceedings of the 2014 IEEE Applied Power Electronics Conference and Exposition—APEC, Fort Worth, TX, USA, 16–20 March 2014; IEEE: Fort Worth, TX, USA, 2014; pp. 2667–2674. [[CrossRef](#)]
26. Deb, K.; Pratap, A.; Agarwal, S.; Meyarivan, T. A fast and elitist multiobjective genetic algorithm: NSGA-II. *IEEE Trans. Evol. Comput.* **2002**, *6*, 182–197. [[CrossRef](#)]
27. Deb, K.; Sindhya, K.; Okabe, T. Self-adaptive simulated binary crossover for real-parameter optimization. In Proceedings of the 9th Annual Conference on Genetic and Evolutionary Computation—GECCO '07, London, UK, 7–11 July 2007; ACM Press: London, UK, 2007; p. 1187. [[CrossRef](#)]
28. Geng, Y.; Wang, T.; Xie, S.; Yang, Y. Analysis and Design of Wireless Power Transfer Systems Applied to Electrical Vehicle Supercapacitor Charge Using Variable-Resistance-Based Method. *Energies* **2022**, *15*, 5867. [[CrossRef](#)]
29. Kim, J.H.; Lee, B.S.; Lee, J.H.; Lee, S.H.; Park, C.B.; Jung, S.M.; Lee, S.G.; Yi, K.P.; Baek, J. Development of 1-MW Inductive Power Transfer System for a High-Speed Train. *IEEE Trans. Ind. Electron.* **2015**, *62*, 6242–6250. [[CrossRef](#)]